

Simple Book Example

TeXstudio Team

January 2013

Contents

1	Theory and methods of plenoptic imaging	1
1.1	Introduction	1
1.2	Plenoptic function and the light field	3
1.3	Plenoptic camera	6
1.4	Plenoptic Camera 1.0	9
1.4.1	Phase space in plenoptic 1.0	14
1.4.2	Light Field Parametrization	16
1.5	Plenoptic 1.0 rendering	21
1.6	Plenoptic Camera 2.0	24
1.7	Plenoptic camera 2.0: a geometrical optics analysis	32
1.8	Plenoptic 2.0 rendering	37
2	Fresnel Simulation Toolbox	39
2.1	Introduction	39
2.2	Scalar Theory of diffraction	40
2.2.1	Helmoltz equation	43
2.2.2	Solutions of Helmholtz Equations	45
2.2.3	The Fresnel Approximation	46
2.3	Operator Free space propagation: Fresnel Approximation approach	47
2.3.1	Multi-Step Fresnel propagation operator	49
2.4	Operator Free space propagation: Angular spectrum of plane waves approach	51
2.4.1	Angular spectrum of plane waves	51
2.4.2	Band Limited Angular Spectrum	55
2.4.3	Corrected Band Limited Angular Spectrum Method	63
2.5	Operator Thin Lens	69
2.5.1	Aliasing in phase sampling	74
2.6	Comparison between the free space propagation operators	76
2.6.1	Description of the system	77
2.6.2	Image of a point source	78

2.6.3	Frequency analysis	81
2.7	Coherence	82
2.7.1	Temporal coherence	84
2.7.2	Spatial Coherence	84
2.7.3	Simulation of spatial coherence	86
2.7.4	Simulation of temporal coherence	91
2.8	Optimization of coherence parameters	92
2.8.1	Optimization of Spatial Coherence	93
2.8.2	Optimization of temporal coherence	96
2.8.3	Coherent imaging vs incoherent imaging	98
3	Simulations of a plenoptic 1.0 system	101
3.1	Description of the system	101
3.1.1	Diffraction effects on the System	103
3.2	Advanced Rendering Techniques	106
3.2.1	Changing Aperture	106
3.2.2	Changing point of view	109
3.3	Depth estimation	110
3.4	Synthetic refocus	115
3.4.1	Synthetic refocus algorithm	117
3.4.2	Shearing Operator	120
3.5	Results of the Simulations	122
3.6	depth estimation through synthetic refocus	127
3.7	Conclusion	130
4	Simulation of a plenoptic 2.0 system	131
4.1	Introduction	131
4.2	Rendering in Plenoptic 2.0	131
4.2.1	Basic Rendering	131
4.2.2	Depth based rendering	131
4.3	Description of the system	131
4.4	Optical performances of a focused plenoptic system	131
4.5	Optical resolution	131
4.5.1	Impulse response ans OTF	131
4.5.2	Two point resolution	131
4.5.3	Optical cut-off frequency	131
4.6	Aberrations	131
5	Light Field Microscope	133
5.1	Introduction	133
5.2	optical setup	133

5.3	Performances of the system	133
5.4	Optical Phase Space	135

List of Figures

1.1	Differences between a traditional camera and a computational camera [1].	3
1.2	Two point representation of light field. Each ray of light if unequivocally defined by the coordinates of two point of interception.	5
1.3	Point angle representation. A ray of light is unequivocally defined by the coordinates of a point that belongs to a plane perpendicular at the optical axis z and by the angles θ_x and θ_y that it forms with the optical axis along the directions x and y	6
1.4	Plenoptic camera and its fundamental components. The presence of the micro array allows to record the light field	7
1.5	Top: Plenoptic camera 1.0. The main lens is focused at infinity, forms and image on the micro array and the micro array are is focused on the sensor. f is the focal length of the main lens and f_μ the focal length of the micro lens array. Bottom: Plenoptic camera 2.0. The main lens is focused at infinity and forms an image on the plane represented by the dashed line. The micro array acts as a relay between the main lens image and the sensor, since it satisfy the lens equation $1/a+1/b = 1/f_\mu$	8
1.6	Ray diagram of a plenoptic 1.0 system. The main lens is in a $2f$ configuration respect the micro array. The sensor plane is conjugated with the main lens plane. The micro lens position maps the position (x,y) of the point P , while the sub image maps the directions of the rays coming from that point. The ray with direction θ_1 falls on the pixel 1 (blue), the ray with direction θ_2 falls on the pixel 2 (green) and the ray with direction θ_3 falls on the pixel 3 (red). The sub image d maps the direction of the ray.	10

1.7	Sampling of Light filed. Each ray is described by a set of four coordinates, two spatial (x,y) and two directional (u,v). The spatial coordinates are sampled by the position of the lens let in the micro array, the directional are sampled by the pixel under the lens let. Point A, its position is sampled by the lens let number 1(x=1), and three rays are green (1,1), red(1,2), blue(1,3). Each ray is defined by x and v. Point B:for one position (x=5) three rays are sampled green (5,1), red(5,2), blue(5,3), dashed line.	12
1.8	F-number matching between the main lens and the micro lens in the array.	13
1.9	When the f-number is matched, all the rays captured by the main lens are mapped on the sub image (yellow).If the f-number is smaller (red), the sub image is smaller and there is an under sampling of the set of rays. If the f-number of the lens let is bigger (green), the sub image is larger and cross talk happens between near sub images	14
1.10	Sampling of the light field and phase space representations of the rays.	15
1.11	Example of a raw plenoptic 1.0 image.	17
1.12	Zoom on the raw image. Each lenslet is formed by 20 by 20 pixel. each pixel represent a direction of the rays hitting the lens let that produced the sub image.	17
1.13	The array view is an array of the different point of view obtained rearranging the pixel according to the directional coordinates.	18
1.14	The array view is an array of the different point of view obtained rearranging the pixel according to the directional coordinates.	19
1.15	Zoom of the central part of the array view showing in detail the different point of views	20
1.16	Sampling of the light field and phase space representations of the rays.[2]	21
1.17	Rendering an image from a plenoptic 1.0 raw data is equal in summing for each position all the directional samples. In figure this process is shown for the the (x, θ_x) slice of the phase space. [3]	23
1.18	rendered image form the raw data in figure 1.11. Resolution is only 75 by 75 pixel.	24

- 1.19 If the main lens image is formed in front of the micro array we have a Copernican configuration, on the top, and the focal length of the micro array is smaller then the distance b . If the main lens image is formed behind the micro array we have a Copernican configuration, on the top, and the focal length of the micro array is bigger then the distance b 26
- 1.20 Raw data of a point source sampled by a plenoptic 2.0 system with a magnification of the micro array stage equal to 0.3. Data acquired with numerical simulations. 28
- 1.21 Zoomed Raw data of a point source sampled by a plenoptic 2.0 system with a magnification of the micro array stage equal to 0.3. Data acquired with numerical simulations. The grid represent the boundaries of each sub image to show how the point of view of the point source changes across the lens lets. The sub images are shifted by a quantity proportional to the position of the lens let in the array. 28
- 1.22 Sampling of the light field by a plenoptic 2.0 system. The one dimensional case is shown. Each micro lens has a diameter equal to d , a focal length f_μ , and images the main lens image on the sensor according to the lens law $1/a + 1/b = 1/f_\mu$. The total range of directions that can be sampled is given by d/b . Each lens let samples a sub set of directions equal to d/a as a single direction. The range of directions shown in red are sampled by the central micro lens as a single point of view. The angular resolution is therefore d/a and the total number of directional sampled is 3. 29
- 1.23 Raw images of a point source simulated with different magnifications. From top left to bottom right: $m = 1$, $m = 0.5$, $m = 0.25$, $m = 0.1$ 31
- 1.24 System formed by a single lens let. The rays at the main lens image plane are transformed into the rays at the sensor plane by the lens let. The transformation can be described by a matrix A 34

1.25	Sampling of the light field by plenoptic 2.0 camera. For each of the two points represented, red and green, The total range of directional coordinates are sampled by three different lens lets. For one position three directions are sampled, with a resolution of d/a . Therefore the directional sampling in plenoptic 2.0 is made across many lens lets. This can be seen in the phase space. Lenset B and C sample 2 directions indicated with the same number in the ray diagram and the phase space. Lens let A only samples one direction of the red point.	36
1.26	Image rendering with the focused plenoptic camera. One pixel of the rendered image is given by the integration on all the directions d/b associated with a given position. The integration takes place across the lens let.	37
2.1	example	46
2.2	To remove the scaling factor between the input and output fields, we developed a multi step Fresnel approach. The field is propagated by unit of dz , the minimum distance to keep the sampling the same.	49
2.3	Structure of the operator free space propagation with the angular spectrum of plane waves method. The initial disturbance $U(x, y; 0)$ is transformed into the angular spectrum $A(f_x, f_y; 0)$ with a Fourier transform implemented by a FFT algorithm. The angular spectrum is multiplied by the propagation transfer function $H(f_x, f_y)$ and the resultant angular spectrum is inverse transformed into the output disturbance $U(x, y; z)$. .	55
2.4	example	57
2.5	example	61
2.6	Structure of the operator free space propagation with the angular spectrum of plane waves method in its band limited version. The initial disturbance $U(x, y; 0)$ is transformed into the angular spectrum $A(f_x, f_y; 0)$ with a Fourier transform implemented by a FFT algorithm. The angular spectrum is multiplied by the propagation transfer function $H(f_x, f_y)$ whose bandwidth has been limited according to equation 2.63. The bandwidth of the transfer function depends by the sampling of the input field, by the wavelength of the light λ and of course by the propagation distance. The resultant angular spectrum is inverse transformed into the output disturbance $U(x, y; z)$.	62

2.7	The maximum spatial frequency is linked to the dimension of the sampling window of the output field w and the propagation distance z	64
2.8	example	67
2.9	Comparison between the Signal to Noise ratio (SNR) as a function of the propagation distance for the three propagation method seen in section 2.4.1. The BL and the corrected BL methods improve the SNR, that instead drops with the increasing of the propagation distance when the normal AS method is used.	68
2.10	Thickness of a lens as a function of position along x coordinate. It can be defined in the same way along the y coordinate . . .	69
2.11	example	71
2.12	A thin lens converts a plane wave into a spherical wave. . . .	73
2.13	Phase profile of a computer generated lens. In Blue it is shown the unfolded quadratic phase term, in red the folded one, subject to aliasing.	74
2.14	Schematic of the 2f system simulated. f is the focal length, z the propagation distances, D is the aperture of the lens, w the field of view and N the sampling resolution.	77
2.15	Operator sequence for the 2f system.	78
2.16	From top to Bottom: Image and intensity cross section of a point source according to multi step method, angular spectrum method, band limited angular spectrum method and corrected band limited angular spectrum method.	80
2.17	From top left to bottom right: Power spectrum of the image of a point source obtained with the multi step Fresnel method, the Angular spectrum method, the band limited angular spectrum method and the corrected band limited angular spectrum method	82
2.18	Young experiment setup.	85
2.19	A random phase mask is generated propagating light coming from an array of sources, each one with a random phase value in the interval $[-\pi, \pi]$	87
2.20	Process of the creation of the phase mask. Top: array of point sources with a random phase value; centre: array of the areas of coherence after the convolution with K ; bottom: randomized areas of coherence after the propagation of d_c	89
2.21	Final random phase mask generated by 10, 50, 100 and 200 sources.	90

2.22	Emission spectrum of the LED considered in our simulations and real image system.	92
2.23	example	93
2.24	Signal to noise ratio of the image of a USAF resolution target plotted as a function of the coherence index C	94
2.25	Images of the USAF resolution target with different values of ι . Increasing the number of point sources generating the phase mask creates improves the resolution and the contrast	95
2.26	Noise due to the speckles ini an image of a USAF resolution target after only 5 iterations.	96
2.27	Images of the USAF resolution target obtained adding an increasing number of snapshot. this is equivalent to increase the integration time of the sensor. As an effect of that the noise due to the speckles caused by the phase mask decreases.	97
2.28	Signal to noise ratio as a function of the number of iterations. The threshold has been calculated looking at the variance of the previous five data.	98
2.29	Comparison between the coherent and an incoherent response of a simple 2f system to a sharp edge.	100
3.1	The parameters that characterize the micro lens array are: the pitch p , defined as the distance between the centres of two neighbours lens lets, the diameter d , the number of lens lets per raw N and the size of the micro array W	102
3.2	The parameters that characterize mi micro lens array are: the pitch p , defined as the distance between the centres of two neighbours lens lets, the diameter d , the number of lens lets per raw N and the size of the micro array W	103
3.3	Values of acceptable lens let diameter to avoid diffraction induced cross talk.	104
3.4	Raw image of a point source.The grid represents the edges of the sub images. If the point source is in focus, it should be represented by only one lens let. Because of diffraction some light goes also on the neighbours sub images.	105
3.5	Phase space of a single point light field: on the left when the condition 3.2 is respected; on the right when diffraction induces cross talk arise between neighbours lens lets. cross talk introduces a blur in the rendered image whose width is Δx	105

3.6	Rendering seen from the (x, θ_x) slice of the phase space. In grey are shown the directional pixels not considered for the integration.	107
3.7	The two images are rendered from the same raw data. The image on the left has been rendered integrating along all the sub image, while the image on the right has been rendered taking only the central pixel form each sub image. Since the object is a 2 dimensional image, the effect on the depth of field is not present.	108
3.8	Raw plenoptic 1.0 image obatined by Marc Levoy. The microscope was a Zeiss Axiovert with a 20x/0.5NA (dry) objective. The microlens array was 24mm x 36mm, with square 125-micron x 125-micron f/20 microlenses, held in front of the Axiovert's side camera port using an optical bench mount. The camera was a Canon 5D full-frame digital SLR. The specimen was the thin silky skin separating two layers of an onion, immersed in oil to improve transparency [4].	109
3.9	Sampling of the light field of a point source in focus, on the top, closer to the main lens, centre, and further away, bottom. When the source is out of focus, both position and directions are sampled by more than one lens let since the main lens image is not formed any more on the lens let plane.	112
3.10	Information on the depth of a point source imaged by a plenoptic 1.0 system. As explained in section 1.4.1 If the point source is in focus, on the top, it's position is sampled by one lens let as well as the whole set of directions	113
3.11	Physical meaning of the slope in the phase space. If the point source is further then the camera focal plane, the phase space line has a negative slope. If the point source is closer then the focal plane, the slope of the phase space line is positive.	114
3.12	Numerical simulation of a point source imaged by a plenoptic 1.0 imaging system. The point source was placed at three different distances from the main lens. On the top we have the focused image. in the centre we have a defocus of 0.125 m far away from the main lens and on the bottom the de focus is 0.25. For these three cases we represent the raw data image, on the left, the rendered image on the center and the phase space line on the left.	115
3.13	The synthetic camera refocusing method is based on the fact that is always possible to define a virtual aperture that is focused on the lens let plane.	116

3.14	Changing the focal plane of the camera is equal to re parametrize the light field according to the new coordinates. The re parametrization is basically a shift proportional to the ratio between the refocused plane and the original camera plane α	118
3.15	Changing the osition of the focal plane is equal to shear the light field in the phase space. The total area remains the same since the total light field is conserved.	121
3.16	Flow chart of the operator shearing.	122
3.17	Set up simulated.	123
3.18	Position of the point sources imaged inside the volume V simulated.	124
3.19	Raw image on the left and rendered image on the right. Intensity is shown in false colour in order to appreciate variations in energy distribution.	125
3.20	Raw image on the left and rendered image on the right. Intensity is shown in false colour in order to appreciate variations in energy distribution.	126
3.21	Refocused images...	126
3.22	Refocused images...	127
3.23	Refocused images...	129
3.24	Estimated values of α represented by blea stars and the theoretical values represented with the blue line.	130
3.25	Distance between the estimated values of alpha and thje actual theoretical values.	130
5.1	The optical momentum correspond to the direction of the ray of light.	135
5.2	136

Chapter 1

Simulations of a plenoptic 1.0 system

In this chapter we present some results obtained simulating raw data images using the simulation platform described in chapter 2. We also describe how we used the digitally generated light fields data to design, develop and test the data processing algorithms, such as the rendering, the synthetic refocus and the depth estimation algorithms. Light fields are generated from the raw images obtained propagating light in the system using the methods described in chapter 2. All the light field processing algorithms use the third parametrization of the light field, described in 1.4.2, that is the four dimensional array of the intensity recorded on the sensor whose indexes are the position x and y , and the the direction θ_x and θ_y .

1.1 Description of the system

The plenoptic 1.0 camera described in section 1.4 has been modelled with a simple $2f$ system composed by a main lens, a micro lens array and a sensor as shown in figure 3.1. The micro lens array is placed at a distance $z = 2f$ from

the main lens, where f is the focal length of the main lens, and the sensor is placed at a distance f_μ from the micro array plane. $z_3 = f_\mu$ is also the focal length of the lens lets. In this configuration the lens let array plane is conjugated with the object plane, while the sensor plane is conjugated with the main lens plane. In order to satisfy the f-number matching condition described in section 1.4, once fixed the propagation distances z_1 , z_2 , z_3 , the resolution N of the input field, the wavelength of the light used and the micro array parameters, the software automatically sets the aperture of the main lens.

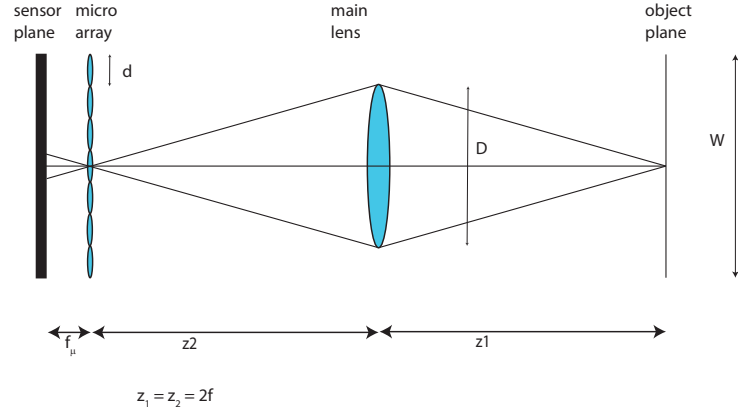


Figure 1.1: The parameters that characterize the micro lens array are: the pitch p , defined as the distance between the centres of two neighbours lens lets, the diameter d , the number of lens lets per raw N and the size of the micro array W .

The micro array parameters are illustrated in figure 3.2. and are the pitch between two close lens lets, the diameter of the single lens let, the number of lens let in a row and the size of the array. In all our simulations the pitch of the lens lets is equal to the size of its diameter and the lens lets are arranged in a square matrix.

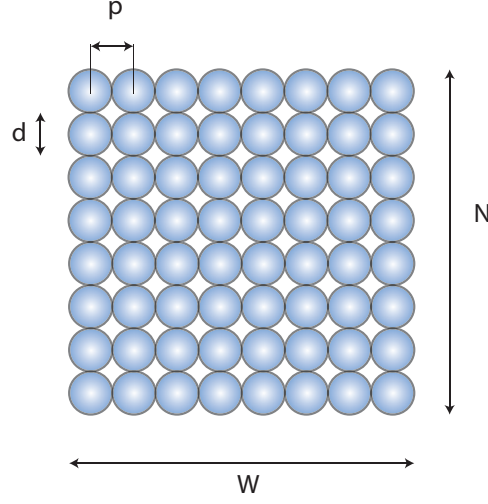


Figure 1.2: The parameters that characterize mi micro lens array are: the pitch p , defined as the distance between the centres of two neighbours lens lets, the diameter d , the number of lens lets per raw N and the size of the micro array W .

1.1.1 Diffraction effects on the System

Diffraction from the lens let circular aperture generates cross talk between neighbours sub images since the light from a single lens let falls in the sub image of the neighbour lens let. This fact generates a blur in the rendered image and a loss of spatial resolution. To avoid this loss of resolution the diameter of each lens let should be larger than the size of its Airy disk diffraction pattern. As seen in equation 2.99 for a lens with a circular aperture, the diameter of the Airy disk at its focal plane is $d = 1.22\lambda z/D$. For the system described the lens let diameter D and z is equal to its focal length f_μ . Therefore the lens let diameter should be at least twice the Airy disk diameter. We have:

$$D > 2.44 \frac{\lambda z}{D} \quad (1.1)$$

Therefore the condition of D is:

$$D > \sqrt{2.44\lambda f_\mu} \quad (1.2)$$

as shown in figure 3.3

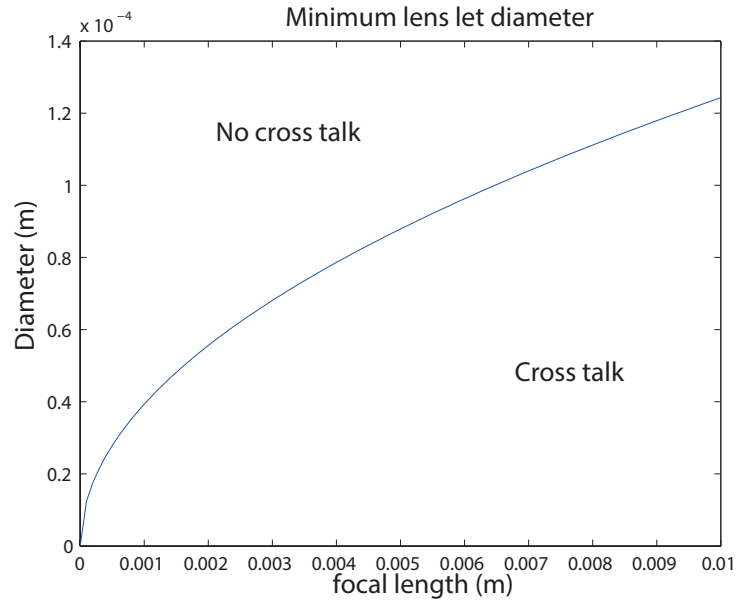


Figure 1.3: Values of acceptable lens let diameter to avoid diffraction induced cross talk.

To conclude this section an example of cross talk raw image is shown. In figure 3.4.

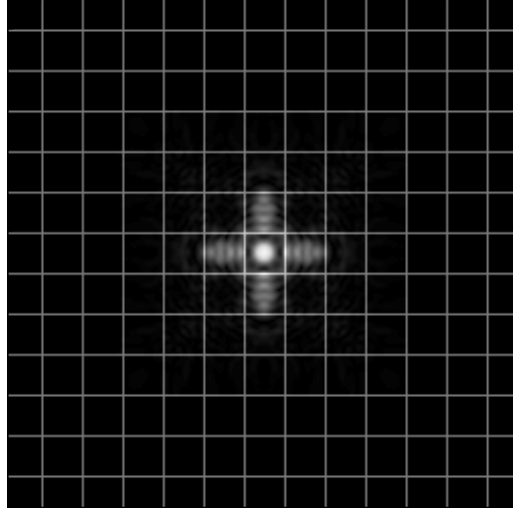


Figure 1.4: Raw image of a point source. The grid represents the edges of the sub images. If the point source is in focus, it should be represented by only one lens let. Because of diffraction some light goes also on the neighbours sub images.

The effects of cross talk are more clear if we analyse the phase space. Figure 3.5 shows the phase space of point source in presence of cross talk, and without cross talk.

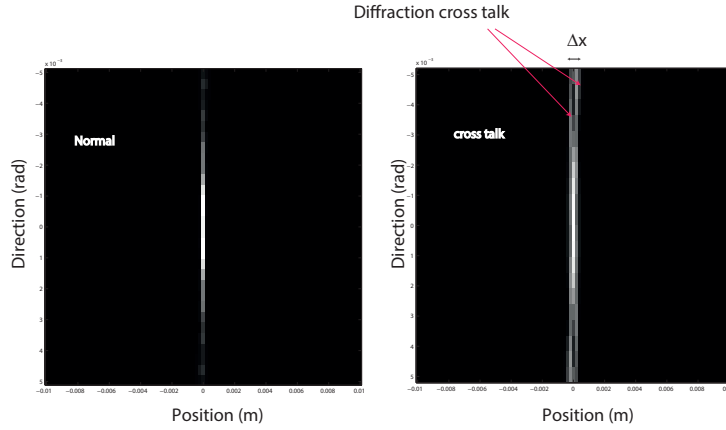


Figure 1.5: Phase space of a single point light field: on the left when the condition 3.2 is respected; on the right when diffraction induces cross talk arise between neighbours lens lets. cross talk introduces a blur in the rendered image whose width is Δx .

1.2 Advanced Rendering Techniques

As described in chapter 1.5, one pixel in the rendered image is obtained as a mean of all the pixels of a sub image. This method generates an image that is equivalent to the image obtained with a conventional camera, without any additional information contained in the light field. In addition to that each lens let sub image generates only one pixel of the final image and the final resolution depends on the number of lens lets in the micro array that is smaller than the resolution that can be obtained by a conventional camera. More advanced forms of enable interesting post processing features. The first two post processing features we present are the change of aperture and the change of point of view. These features are achieved integrating the each sub image along a sub set of directional coordinates, that correspond to a smaller number of pixels.

1.2.1 Changing Aperture

The possibility to change the aperture of the main lens in post processing is a very interesting feature. The quality of the image captured by a conventional camera depends, with a lot of simplifications, by the combination of shutter speed and aperture chosen in order to get the optimum total exposure [23]. In our simulations the shutter speed is not an issue since all the objects imaged where static with constant and uniform illumination. Therefore what determine the exposure is the aperture of the main lens or the f number. The f number is proportional to the depth of field of the imaging system that can be defined as the range of depths that appears sharp in the resulting photograph

[2]. If the f number increases and the aperture gets smaller, the depth of field increases. Therefore a plenoptic camera can control the depth of field in post processing. If we look at the raw plenoptic image, each sub image is formed by a number of samples of the directions of the rays. If in equation 1.6 we reduce the range of integration along the directional coordinates, this is equivalent in reducing the aperture of the main lens, since less rays will be considered to form the intensity of each pixel. The result is a rendered image that looks like it has been captured with a narrower aperture, therefore with less light. From a computational point if we want to reduce the aperture of a k pixels we have:

$$I(x, y) = \frac{1}{N'^2} \sum_{i=k/2}^{N-k/2} \sum_{j=k/2}^{N-k/2} L(x, y, i, j) \quad (1.3)$$

where $N' = N - k$. This operation in the phase space is shown in figure:

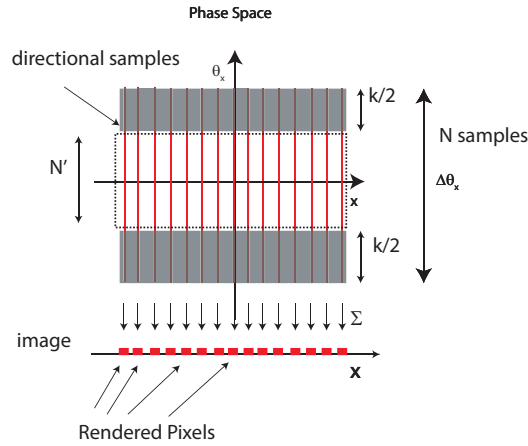


Figure 1.6: Rendering seen from the (x, θ_x) slice of the phase space. In grey are shown the directional pixels not considered for the integration.

An example of implementation of the change of the aperture can be seen in figure 3.7. The two images has been rendered from the raw data described

in section 1.4.2. Two examples of imaged rendered changing the aperture in post processing can be seen in figure 3.7.

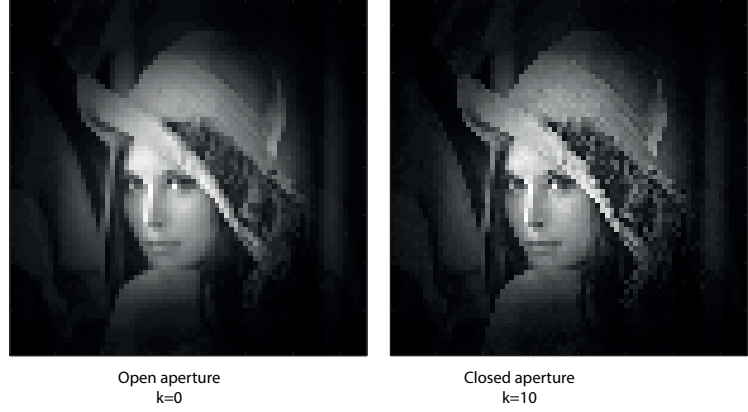


Figure 1.7: The two images are rendered from the same raw data. The image on the left has been rendered integrating along all the sub image, while the image on the right has been rendered taking only the central pixel from each sub image. Since the object is a 2 dimensional image, the effect on the depth of field is not present.

The object, as explained in section 1.5, is a two dimensional picture, the extended depth of field is not noticeable. What can be quantified is the amount of light present in the two images. With full aperture we have a total intensity of NUMBER and a mean intensity of NUMBER, while with the smallest aperture the total intensity and the mean intensity are respectively:NUMBER AND NUMBER. As expected the total amount of light decrease if we close the aperture, even in the post processing case. Regarding the extended depth of field achievable reducing the aperture in post processing to a single ppxel, applied the home made algorithm to raw data downloaded from Stanford microscopy group.

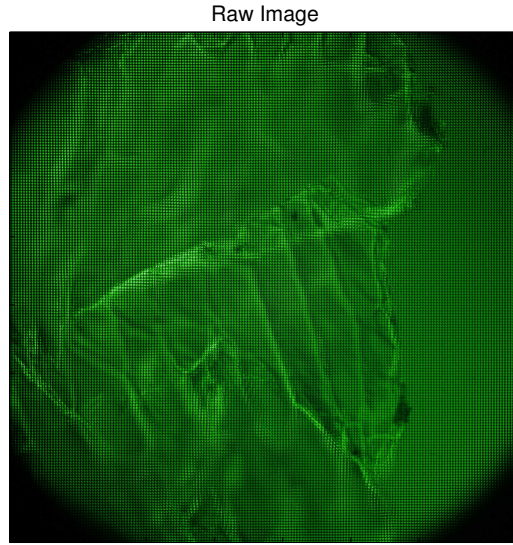


Figure 1.8: Raw plenoptic 1.0 image obtained by Marc Levoy. The microscope was a Zeiss Axiovert with a 20x/0.5NA (dry) objective. The microlens array was 24mm x 36mm, with square 125-micron x 125-micron f/20 microlenses, held in front of the Axiovert's side camera port using an optical bench mount. The camera was a Canon 5D full-frame digital SLR. The specimen was the thin silky skin separating two layers of an onion, immersed in oil to improve transparency [4].

1.2.2 Changing point of view

Selecting the directional components to integrate is possible to change to point of view of the rendered image, in the limit of the directions contained in the f-number of the main lens. Viewpoint can be chosen both in x and y direction. It is possible to choose only one specific viewpoint (θ_x, θ_y) , that rendering the image using only one single pixel per sub image, as shown in figure, or it is possible to select a point on view in θ_x or θ_y and integrate over

all the other direction. The rendering equation then becomes:

$$\begin{aligned}
 I(x, y) &= \frac{1}{N} \sum_{i=0}^N L(x, y, i, \theta_y) \\
 I(x, y) &= \frac{1}{N} \sum_{j=0}^N L(x, y, \theta_x, j)
 \end{aligned} \tag{1.4}$$

1.3 Depth estimation

In this section we will explain how it is possible to extract depth information from light fields data. In the specific case of plenoptic 1.0 raw data, depth can be decoded looking at the phase space. In section 1.4.1 is explained that a point source on the focal plane of the main lens looks like a straight vertical line in the phase space. The physical meaning of this is that for a single position, one lens let, all the directional coordinates are sampled. If the point source is out of focus the situation is different. If the source is closer to the main lens respect the focal plane, it will be imaged on a plane that is behind the micro array. This situation is shown in figure 3.9 in the middle. Both directional and positional coordinates are sampled by more than one lens let. Each sub image will sample a set of directional coordinates correspondent to the part of the main lens that is being imaged. In figure 3.10 it is shown what happens in the phase space. On the lens let plane the spot size will have a width of Δx proportional to the distance, therefore the directions will be sampled by the lens lets included in this interval. Each lens let receive light coming from a particular area of the main lens, its correspondent sub image only records the pixels linked with those coordinates as can be seen comparing figure 3.9 with figure 3.10. The resultant phase space representation is still a straight line, but with positive

slope proportional to the distance of the point source 3.10. If the source is further away from the plane where the main lens is focused, the main lens image is formed before the lens lets plane. The point is still sampled by more than one lens let included in the spot size Δx . The difference with the previous case is that now in the phase space the point source is represented by a straight line with a negative slope. The physical meaning of the slope of the phase space line can be understood looking at figure 3.11. When the main lens image is formed in front of the micro lens plane, if the increasing directions on the θ_x are mapped on decreasing positions in the x plane therefore the line on the phase space representing the point has a negative slope. If the image is formed behind the micro lens plane the image is this inversion is absent and the line in the phase space has a positive slope [2]. This characteristic of the phase space permits to discriminate between points in the scene that are in front or behind the main lens focal plane, giving a first rough depth estimation.

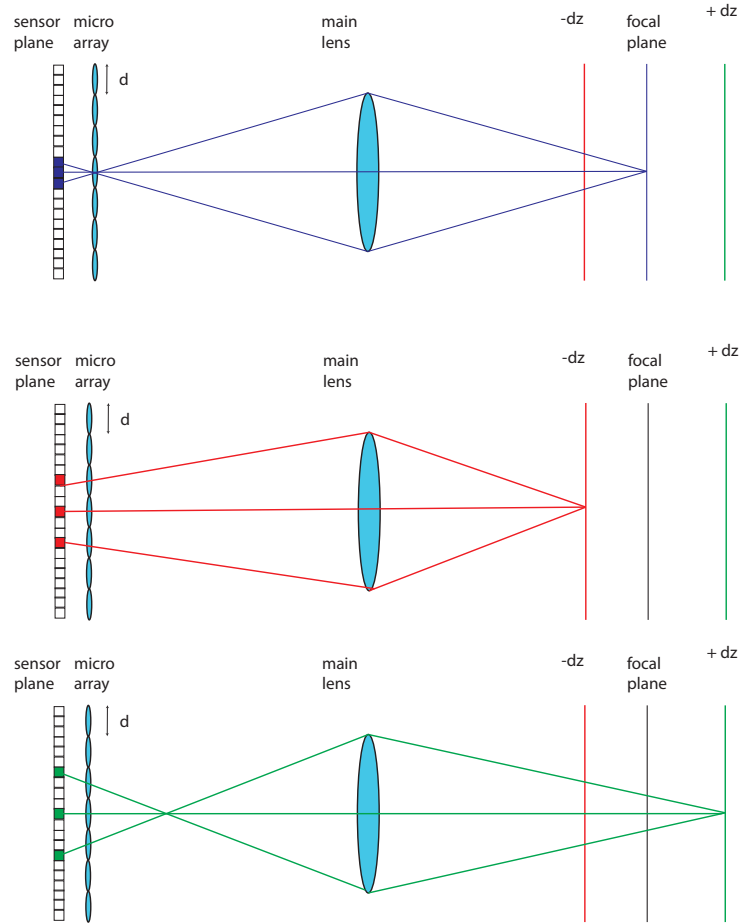


Figure 1.9: Sampling of the light field of a point source in focus, on the top, closer to the main lens, centre, and further away, bottom. When the source is out of focus, both position and directions are sampled by more than one lens let since the main lens image is not formed any more on the lens let plane.

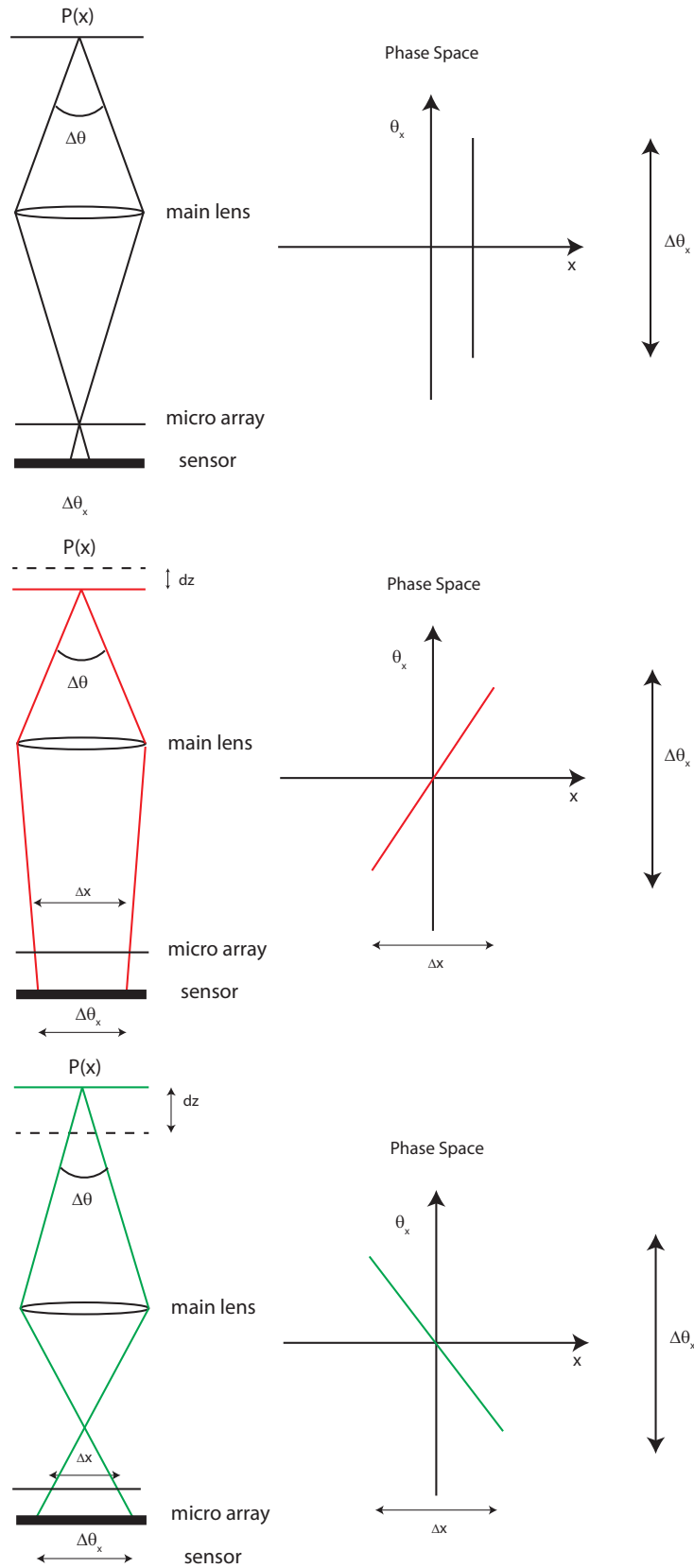


Figure 1.10: Information on the depth of a point source imaged by a plenoptic 1.0 system. As explained in section 1.4.1 If the point source is in focus, on the top, it's position is sampled by one lens let as well as the whole set of directions .

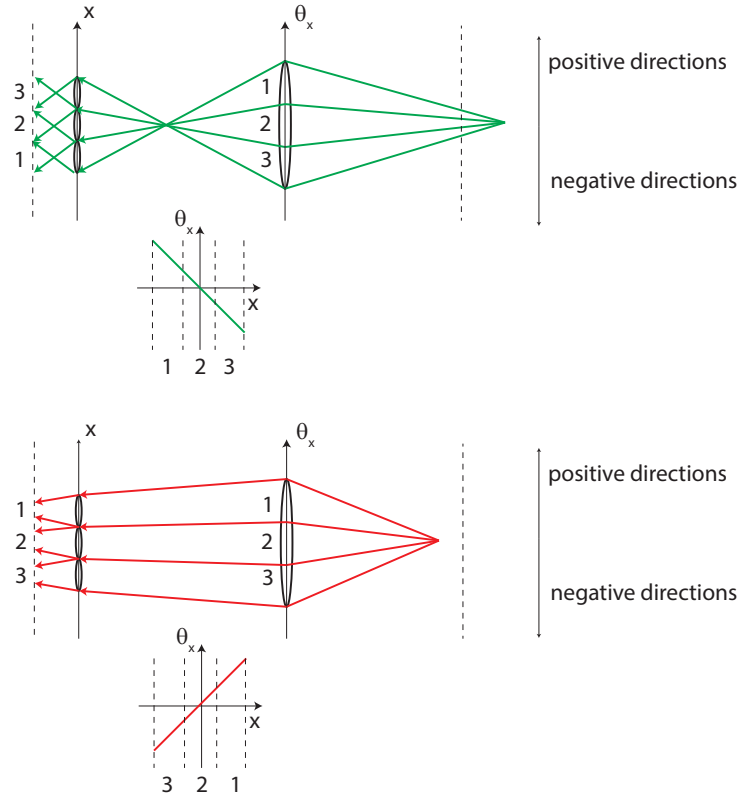


Figure 1.11: Physical meaning of the slope in the phase space. If the point source is further then the camera focal plane, the phase space line has a negative slope. If the point source is closer then the focal plane, the slope of the phase space line is positive.

A simulation of plenoptic 1.0 camera has been made to verify this fact. The system was composed by a main lens with a focal length of 120 mm , in a $2f$ configuration creating an image on the micro array plane. The Micro lens array

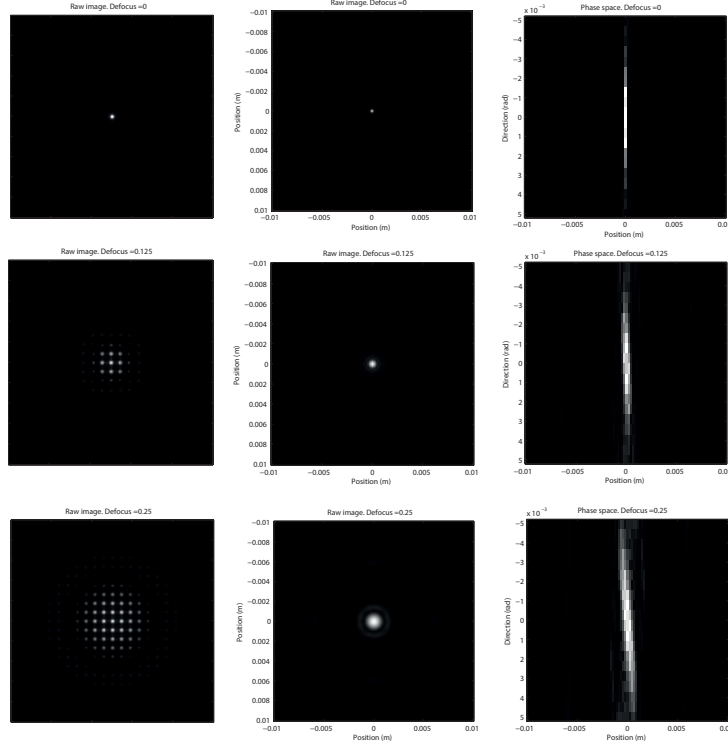


Figure 1.12: Numerical simulation of a point source imaged by a plenoptic 1.0 imaging system. The point source was placed at three different distances from the main lens. On the top we have the focused image. in the centre we have a defocus of 0.125 m far away from the main lens and on the bottom the de focus is 0.25. For these three cases we represent the raw data image, on the left, the rendered image on the center and the phase space line on the left.

1.4 Synthetic refocus

To conclude this chapter we examine one of the most fascinating post processing features enabled by collecting the light field is possibility to refocus an image after it has been captured. This features is called synthetic refocusing and is based on the fact that the recorded light field can be used to compute images as if they were taken by a synthetic camera positioned and focused differently from the actual camera. In this section we will explain the

method to manipulate light field to refocus in post processing an image. We will also show how this method, based on a synthetic camera model obtained with ray tracing, can be implemented in a wave optics approach, and we will discuss the limitations and the issues arising from a wave approach respect the simple and ideal ray optics approach. This method is based on the fact that it is possible to define a synthetic camera composed by an aperture and a sensor plane, for which the defocused object plane results in focus. Referring to figure 3.13, the main lens produces an out of focus image on the micro lens plane. The directional set of coordinates Δu is mapped by along the range of spatial coordinates Δx . The light field can be reparametrized in terms of a synthetic light field generated by a synthetic aperture, represented by the dashed lens, that focuses the object on a synthetic focal plane, represented by the dashed line. This second light field is parametrized with the coordinates $u' v'$ and $x' y'$.

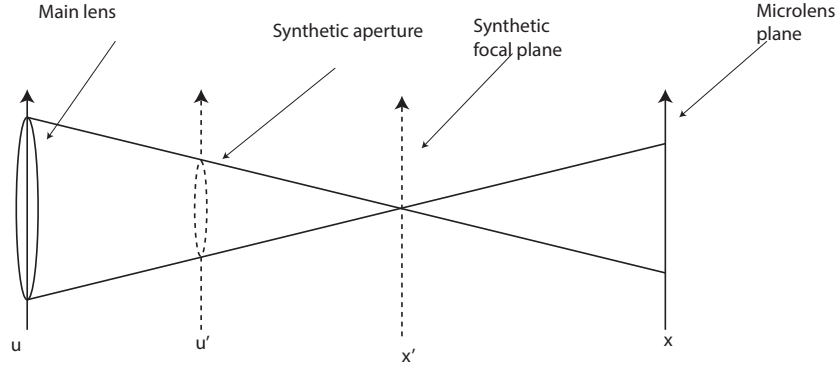


Figure 1.13: The synthetic camera refocusing method is based on the fact that it is always possible to define a virtual aperture that is focused on the lens plane.

Following the work of Ng *et al.* [10] and in analogy with what explained in section 1.5, we define the intensity obtained rendering a synthetic light

field $L'(x', y', u', v')$ parametrized by the synthetic planes (x', y') and (u', v') as:

$$I(x, y) = \iint L'(x', y', u', v') A(u', v') du' dv' \quad (1.5)$$

The goal is to express this intensity as a function of the captured light field $L(x, y, u, v)$ finding the relationship that links the set of coordinates x, y, u, v with the coordinates x', y', u', v' .

1.4.1 Synthetic refocus algorithm

Changing the focal plane is equal to change the distance between the main lens and the sensor. Therefore correctly refocus an image there is no need to shift the main lens plane or changing the aperture, and we can do the following simplifications:

- We assume that to refocus an object, only the synthetic sensor plane x', y' will be moved. Therefore the main lens plane u', v' is at the same position of the plane u, v , and no transformation is performed on the directional coordinates, so we can write $(u, v) = (u', v')$.
- the aperture of the main lens will not change, $A(x', y') = 1$.

In figure 3.14 is shown a two dimensional diagram explaining the re parametrization under the hypotheses explained above. The diagram only shows the coordinates x and u , and the y and v dimensions share an identical relationship. F is the distance of the main lens from the lens let array plane, and F' is the distance from the synthetic focal plane. We define the parameter α as the ratio between these two distances:

$$\alpha = \frac{F}{F'} \quad (1.6)$$

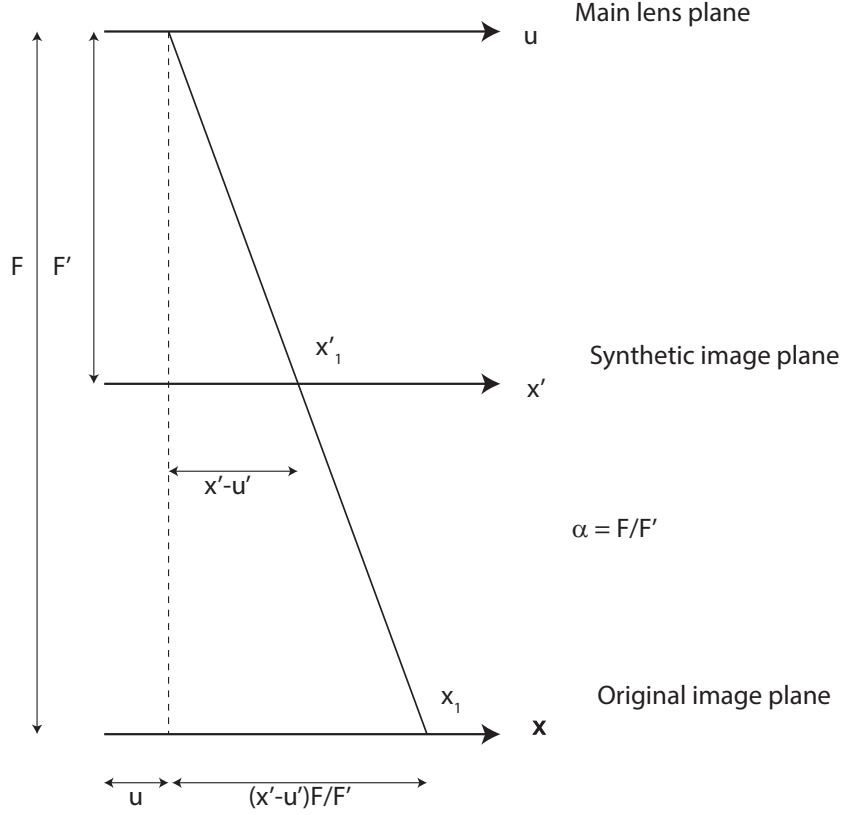


Figure 1.14: Changing the focal plane of the camera is equal to reparametrize the light field according to the new coordinates. The reparametrization is basically a shift proportional to the ratio between the refocused plane and the original camera plane α .

The factor α can be:

- $\alpha = 1$ when the synthetic focal plane is at the same position of the main lens focal plane
- $\alpha > 1$ when the distance between the main lens and the synthetic image plane is smaller than the distance between the main lens and its original focal plane. This occurs when we are refocusing on a plane that is further away from the main lens focal plane.

- $\alpha < 1$ when the distance between the main lens and the synthetic image plane is bigger than the distance between the main lens and its original focal plane. This occur when we are refocusing on a plane that it closer to the main lens.

A ray of light that crosses the main lens plane at the coordinate u and that then intercepts the synthetic image plane at the point x'_1 , can be represented using with the coordinates of the original image plane x_1 . Because of similar triangles, the value of the x coordinate on the image plane can be expressed as a function of the coordinates u, x' . We have:

$$x_1 = u + (x'_1 - u) \frac{F}{F'} = u + (x'_1 - u) \alpha \quad (1.7)$$

Therefore extending to the four dimensional case, the points belonging to the synthetic image plane can be expressed as function of the directional coordinates at the main lens plane and the spatial coordinates at the original image plane as:

$$\begin{aligned} x' &= \frac{x}{\alpha} + u \left(1 - \frac{1}{\alpha}\right) \\ y' &= \frac{y}{\alpha} + v \left(1 - \frac{1}{\alpha}\right) \end{aligned} \quad (1.8)$$

With this change of coordinates the light field at the synthetic focal plane x' can be written substituting equations 3.8 into equation 3.5.

$$I(x, y) = \iint L \left(\frac{x}{\alpha} + u \left(1 - \frac{1}{\alpha}\right), \frac{y}{\alpha} + v \left(1 - \frac{1}{\alpha}\right), u, v \right) A(x', y') du dv \quad (1.9)$$

Equation 3.9 represent the rendered image obtained integrating along the directional coordinates the light field re parametrized as if it were captured by a camera whose focal plane is the same as the synthetic focal plane.

Focusing at different depths corresponds to changing the separation between the lens and the film plane, resulting in a shearing of a factor α the four dimensional the light field recorded at the micro array plane. The shearing of the light field can be seen as the composition of two transformations:

- a scaling due to the factor α that depends by the distance of the synthetic focal plane from the main lens.
- a translation term $u(1 - 1/\alpha)$ that increases with the directional coordinates and with the magnitude of the factor alpha.

The synthetic light field is therefore obtained shifting and rescaling by a factor α the light field captured by the camera and the effects of synthetic refocus can be described by a linear operator acting on the four dimensional light field

1.4.2 Shearing Operator

The synthetic refocus equation 3.9 has been obtained with ray optics considerations only. However, it can be applied to light fields obtained light fields obtained with wave optics simulations. The only difference will be that particular attention should be given in the design of the imaging system in order to avoid cross talk effects induced by diffraction, as explained in section 3.1.1. The effects of this operator in the phase space is a change of the slope of the lines describing the points of the image in the phase space. Since the total light field is conserved, the area in the phase space remains the same, hence the projection of the light field on the phase space results sheared respect the original one.

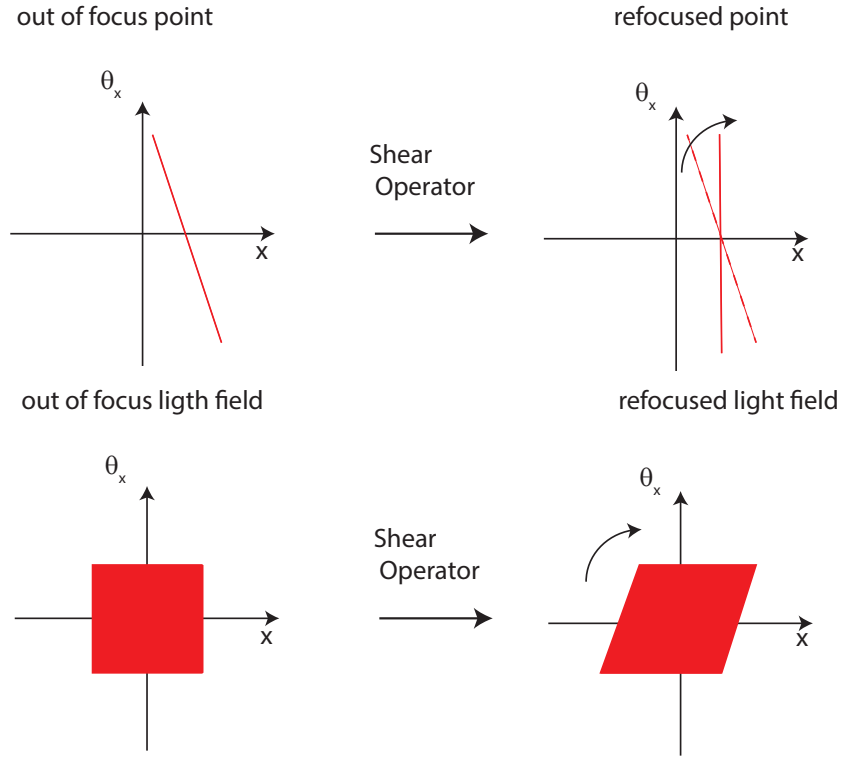


Figure 1.15: Changing the position of the focal plane is equal to shear the light field in the phase space. The total area remains the same since the total light field is conserved.

From a computation point of view we implemented the synthetic refocus operator in MATLAB. The operator is composed by three stages. The first stage it creates a new set of spatial coordinates shifting and rescaling the the original set of coordinates as shown in equation 3.8. Then the output synthetic light field is created interpolating the input light field using as a base the new set of coordinates. The flow chart can be seen in figure 3.16

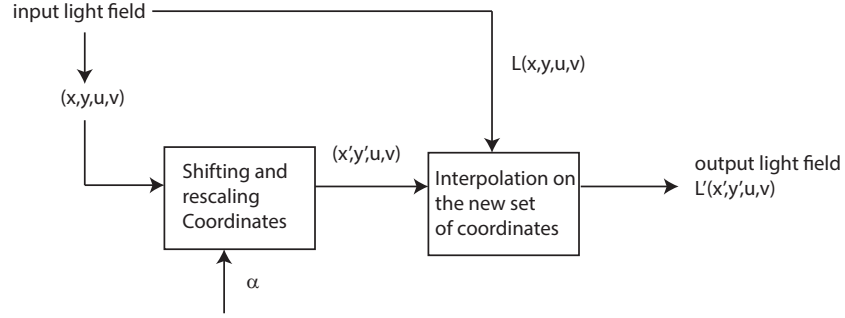


Figure 1.16: Flow chart of the operator shearing.

1.5 Results of the Simulations

To test and explore the potentials of the synthetic refocusing algorithm we generated a set of light field using the wave optics simulation toolbox described in section ?? . The System simulated is tha one described in section 2.6.1 and shown in figure 3.17 and the optical parameters can be found in the following table.

Main lens focal length f	120mm
Lens aperture D	3.6 mm
Micro lens focal length f_{μ}	10 mm
Micro lens diameter d	150 μm
Micro array pitch p	150 μm
Field of view W	20 mm
f-number	33.6
sensor resolution	3030 by 3030 pixel

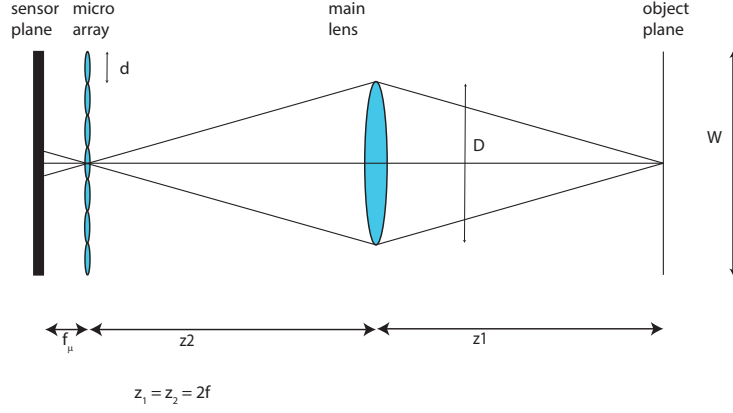


Figure 1.17: Set up simulated.

With this set up the final rendered image resolution is of 101 by 101 pixel. Each pixel of the final image corresponds to a lens let, therefore the spatial resolution in the final image is equal to the diameter of the single lens let. Each sub image has 30 by 30 lens let, meaning that the full set of directional coordinates is sampled by $N_{sub} = 30$ pixels. The angular resolution is therefore given by:

$$\delta\theta = \frac{\Delta\theta}{N_{sub}} = \frac{NA}{N_{sub}} \quad (1.10)$$

and is equal to $\delta\theta = 2.5 \times 10^{-4} \text{ rad}$. The first object to be imaged was a volume V of dimension 20 mm x 20 mm x 100 mm containing three point sources. Each point source has been simulated by a circle of 10 μm diameter and are positioned as shown in figure 3.18

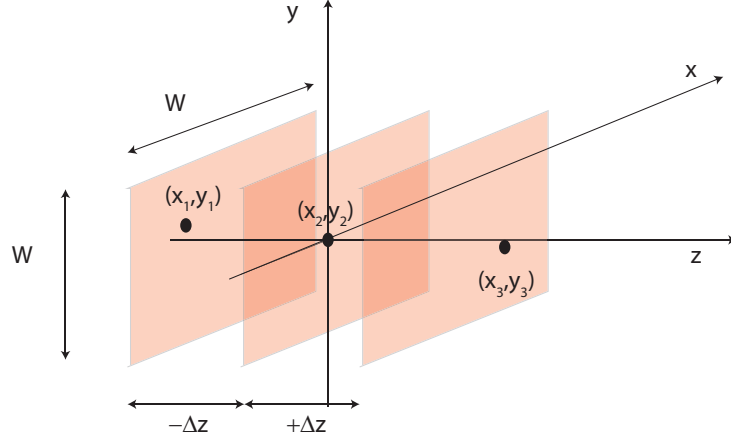


Figure 1.18: Position of the point sources imaged inside the volume V simulated.

Each plane has been imaged singularly setting the distance z_1 equal to the sum of the distance of the main lens focal plane and the defocus δz . The Coordinates of the points where:

- A: $x_1 = -3mm, y_1 = -3mm, z_1 = -50mm$
- B: $x_2 = 0mm, y_2 = 0mm, z_2 = 0mm$
- C: $x_3 = +3mm, y_3 = +3mm, z_3 = +50mm$

After that the light of the three planes has been propagated into the system, the final raw image has been obtained summing the three separate raw images normalized by the total amount of energy contained. This can be made possible since the Fresnel simulation toolbox is time independent. In figure are shown the total raw image and the rendered image integrated without any refocusing. 3.18

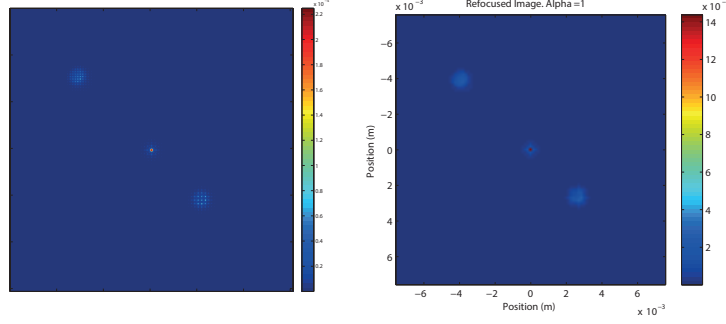


Figure 1.19: Raw image on the left and rendered image on the right. Intensity is shown in false colour in order to appreciate variations in energy distribution.

For a defocus of 50 mm the factor alpha can be obtained using reversing the lens equation. For the 2f system simulated and referring to figure 3.14 for notations, we have

$$\frac{1}{f} = \frac{1}{F'} + \frac{1}{z + \Delta z} \quad (1.11)$$

Since $\alpha = F/F'$, and in a 2f system $F=2f=z$, we have:

$$\frac{1}{f} = \frac{\alpha}{2f} + \frac{1}{2f + \Delta z} \quad (1.12)$$

Resolving for α we have:

$$\alpha = \frac{2f + s\Delta z}{2f + \Delta z} \quad (1.13)$$

In figure are shown the values of α obtained by equation 3.13 for defocus values varying between plus and minus 10 cm.

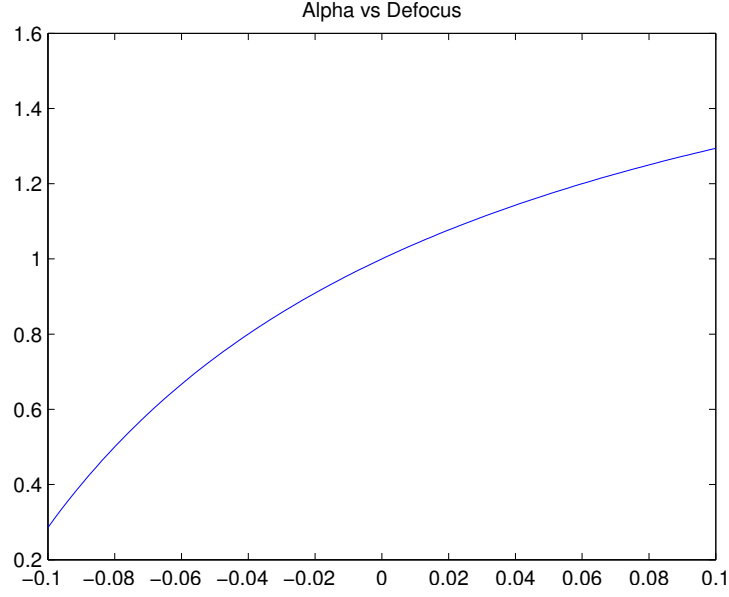


Figure 1.20: Raw image on the left and rendered image on the right. Intensity is shown in false colour in order to appreciate variations in energy distribution.

We can see from figure 3.20 that it is not linear with defocus, and therefore the axial resolution is not linear. To conclude this section we show the refocused images obtained shearing the light field extracted by the raw image in figure 3.19. According to equation 3.13, the point A is refocused for a value of α equal to 0.7 and point B for $\alpha = 1.17$. Results are shown in figure 3.21

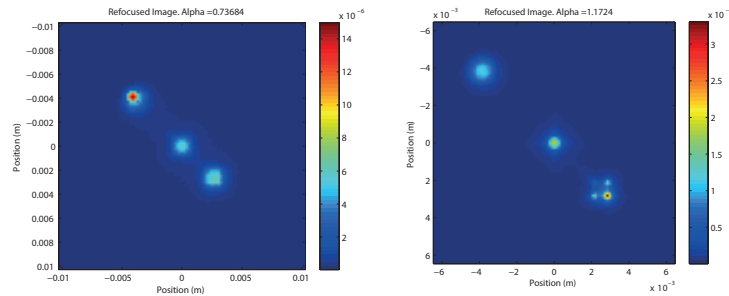


Figure 1.21: Refocused images...

1.6 depth estimation through synthetic refocus

The synthetic refocus algorithm provides a method to estimate the depth of a point source in a volume. If we have a look at the Fourier transform of a rendered image of a point source before and after refocus, we note that when the point source is in focus, its spectrum is broader than the blurred one. This fact is true for normal images as well, when the presence of more sharp details in the in focus image, causes its spectrum to have a larger amount of high spatial frequencies. Inj figure is shown the difference between the spectrum of the out of focus image(blue) and the in focus image(red) for a defocus of 5 cm.

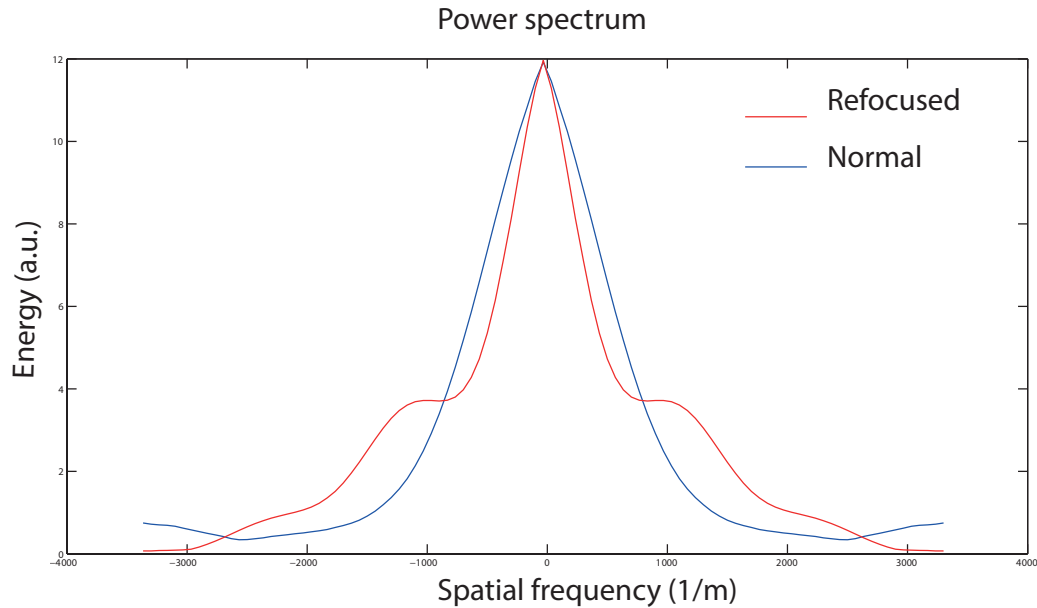


Figure 1.22: Refocused images...

The action of shearing the light field produces a redistribution of the power spectrum of the signal towards high frequency. This effect causes the

sharpness of the image and therefore the refocus. This effect can be used to estimate the depth of object imaged just evaluating its level of blur. The method consist in creating a focal stack shearing the light field at different values of the coefficient alpha, that correspond to different focal planes, and rendering the images. After the focal stack is created the power spectrum of each image is calculated using the fast Fourier transform algorithm. It is then removed the low frequency terms and it calculated the total energy contained in the high frequency term. Plotting the values of energy as a function of the different alpha coefficients, we obtain a curve with presents a maximum in the proximity of the most in focus image. This maximum corresponds to the value of alpha that best estimates the actual value of alpha. In figure 3.23 are shown the energy as a function of the refocus parameter alpha for a point source placed at different depths. The vertical red line indicate the position of the maximum. The values of the estimated alpha and the real one are shown in the following table:

Estimated α	Real α	Error	Defocus
0.85	0.738	0.1132	-0.05 m
0.925	0.8837	0.0413	-0.025 m
1.080	1.0943	-0.0143	+0.025 m
1.105	1.1724	0.0674	+0.05 m

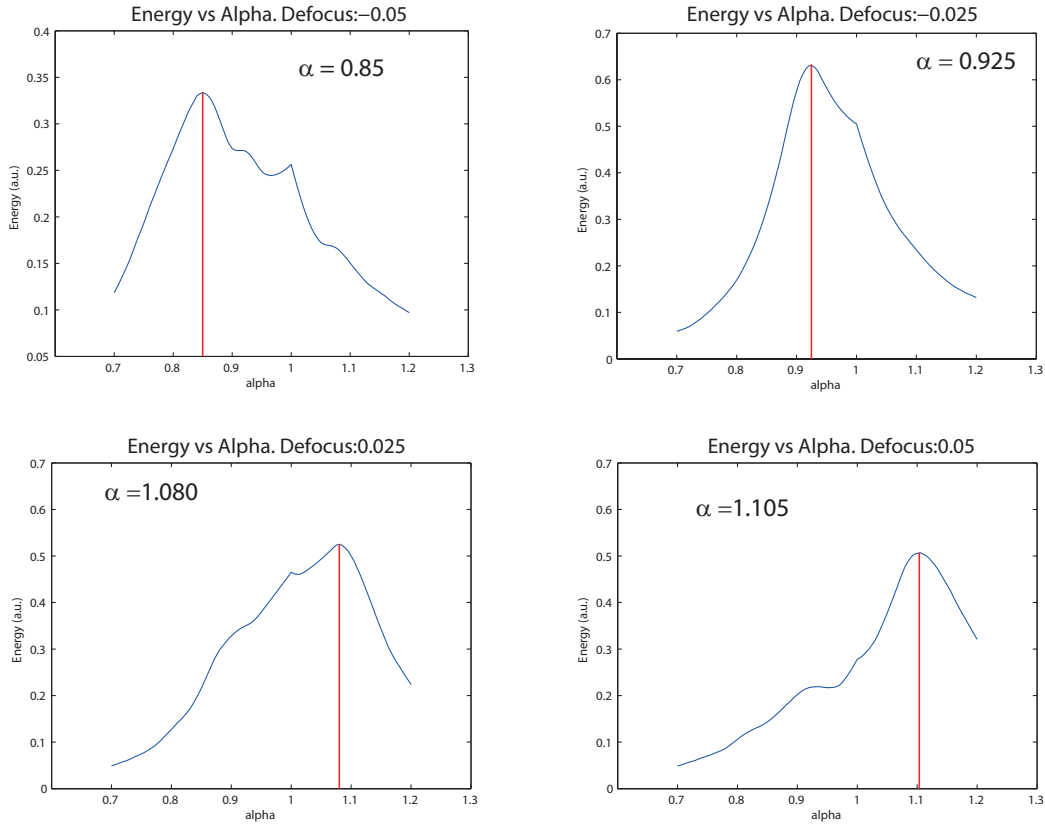


Figure 1.23: Refocused images...

In figure are shown the distribution of the estimated values of α in comparison with the actual values of α from equation 3.13. It is clear that when the object is close to the main lens, defocus is negativ, the error in evaluating α is bigger, while the more accurate values are in the range of depth close to the focal plane.

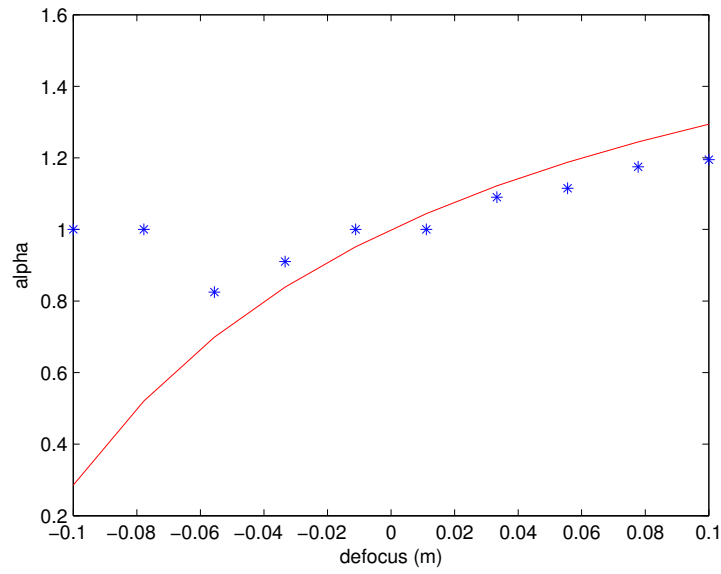


Figure 1.24: Estimated values of α represented by blue stars and the theoretical values represented with the red line.

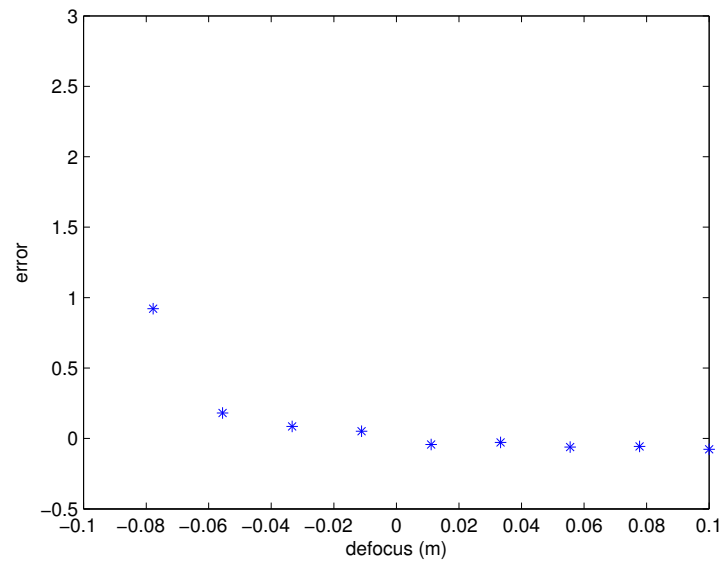


Figure 1.25: Distance between the estimated values of α and the actual theoretical values.

1.7 Conclusion

Bibliography

- [1] Shree K Nayar. Computational cameras: Redefining the image. *Computer*, (8):30–38, 2006.
- [2] Ren Ng. *Digital light field photography*. PhD thesis, stanford university, 2006.
- [3] Todor Georgiev and Andrew Lumsdaine. Focused plenoptic camera and rendering. *Journal of Electronic Imaging*, 19(2):021106–021106, 2010.
- [4] Levoy Mark. Stanford light field microscope project, 2005.
- [5] Changyin Zhou and Shree K Nayar. Computational cameras: Convergence of optics and processing. *Image Processing, IEEE Transactions on*, 20(12):3322–3340, 2011.
- [6] Edward H Adelson and James R Bergen. *The plenoptic function and the elements of early vision*. Vision and Modeling Group, Media Laboratory, Massachusetts Institute of Technology, 1991.
- [7] Edward H Adelson and John Y. A. Wang. Single lens stereo with a plenoptic camera. *IEEE Transactions on Pattern Analysis & Machine Intelligence*, (2):99–106, 1992.

- [8] Marc Levoy and Pat Hanrahan. Light field rendering. In *Proceedings of the 23rd annual conference on Computer graphics and interactive techniques*, pages 31–42. ACM, 1996.
- [9] Todor Georgiev and Chintan Intwala. Light field camera design for integral view photography. *Adobe System, Inc*, 2006.
- [10] Ren Ng, Marc Levoy, Mathieu Brédif, Gene Duval, Mark Horowitz, and Pat Hanrahan. Light field photography with a hand-held plenoptic camera. *Computer Science Technical Report CSTR*, 2(11), 2005.
- [11] Andrew Lumsdaine and Todor Georgiev. Full resolution lightfield rendering. *Indiana University and Adobe Systems, Tech. Rep*, 2008.
- [12] Andrew Lumsdaine and Todor Georgiev. The focused plenoptic camera. In *Computational Photography (ICCP), 2009 IEEE International Conference on*, pages 1–8. IEEE, 2009.
- [13] Victor Guillemin and Shlomo Sternberg. *Symplectic techniques in physics*. Cambridge University Press, 1990.
- [14] Arnold Sommerfeld. Optics lectures on theortical physics, vol. iv. *Optics Lectures on Theortical Physics, Vol. IV by Arnold Sommerfeld New York, NY: Academic Press INC, 1954*, 1, 1954.
- [15] Joseph W Goodman. *Introduction to Fourier optics*. Roberts and Company Publishers, 2005.
- [16] Maciej Sypek. Light propagation in the fresnel region. new numerical approach. *Optics communications*, 116(1):43–48, 1995.

- [17] Rafael C Gonzalez, Richard Eugene Woods, and Steven L Eddins. *Digital image processing using MATLAB*. Pearson Education India, 2004.
- [18] Kyoji Matsushima and Tomoyoshi Shimobaba. Band-limited angular spectrum method for numerical simulation of free-space propagation in far and near fields. *Optics express*, 17(22):19662–19673, 2009.
- [19] Maciej Sypek. Reply to the comment on “light propagation in the fresnel region—new numerical approach”. *Optics Communications*, 282(6):1074–1077, 2009.
- [20] Max Born and Emil Wolf. *Principles of optics: electromagnetic theory of propagation, interference and diffraction of light*. Cambridge university press, 1999.
- [21] Joseph W Goodman and Randy L Haupt. *Statistical optics*. John Wiley & Sons, 2015.
- [22] Emil Wolf. *Introduction to the Theory of Coherence and Polarization of Light*. Cambridge University Press, 2007.
- [23] Frank L Pedrotti and Leno S Pedrotti. Introduction to optics 2nd edition. *Introduction to Optics 2nd Edition by Frank L. Pedrotti, SJ, Leno S. Pedrotti New Jersey: Prentice Hall, 1993*, 1, 1993.
- [24] Kurt Bernardo Wolf. *Geometric optics on phase space*. Springer Science & Business Media, 2004.